DOI: 10.1021/ma100278q

Macromolecules
ARTICLE

Electric Field Induced Gyroid-to-Cylinder Transitions in Concentrated Diblock Copolymer Solutions

Kristin Schmidt,[†] Christian W. Pester,[§] Heiko G. Schoberth,[‡] Heiko Zettl,[‡] Kerstin A. Schindler,[‡] and Alexander Böker*[,§,⊥]

[†]*Materials Research Laboratory, University of California, Santa Barbara, California 93106,* [‡]*Physikalische Chemie II, Universität Bayreuth, D-95440 Bayreuth, Germany,* [§]*DWI an der RWTH Aachen e.V., Lehrstuhl für Makromolekulare Materialien und Oberflächen, RWTH Aachen University, D-52056 Aachen, Germany, and* [⊥]*JARA-FIT, RWTH Aachen University, D-52056 Aachen, Germany*

Received February 5, 2010; Revised Manuscript Received March 31, 2010

ABSTRACT: Block copolymers show a variety of microdomain structures due to their ability to phase separate. The bicontinuous gyroid phase and its behavior under the influence of external fields are particularly interesting with regard to technological applications. In this paper, we studied the behavior of a gyroid-forming block copolymer solution under the influence of an external electric field. As a model system, we used a solution of polystyrene-*b*-polyisoprene in toluene. We will show that the gyroid phase can be aligned by a moderate electric field and can be forced to undergo a phase transition to the cylindrical phase under a sufficiently high electric field. This process is reversible, and the cylinders immediately reconnect after the electric field is switched off, generating a highly aligned gyroid phase.

Introduction

One of the most fascinating properties of block copolymers is their ability to phase separate into periodic microdomain structures, such as the body-centered-cubic crystal of spherical domains (S), hexagonally packed cylinders (C), bicontinuous gyroid (G), and lamellar domains (L). The study of the phase diagram of various block copolymer systems and the respective theoretical prediction have attracted great interest since the 1980s. Here, mean-field theories, such as the Ginzburg−Landau type model with the random phase approximation (RPA) and the self-consistent-field theory (SCFT), have been successfully applied.[1−6]

By far the most prominent complex phase is the gyroid phase, a bicontinuous cubic structure with $Ia\bar{3}d$ symmetry, in which the minority domain forms interweaving left- and right-handed 3-fold coordinated lattices. These interpenetrating networks will lead to nontrivial rheological properties due to very complex possible topological transformations under external fields. As a result, the gyroid morphology is of great interest for applications in chemical engineering, such as three-dimensional photonic crystals, microporous systems, nanoreactors, etc.[7−9] A detailed knowledge on how the gyroid structure would respond to different types of external influences, like temperature change or various possible external fields, is required. In addition, for most applications a large-scale well-ordered gyroid structure is necessary. However, a fundamental understanding of the gyroid structure is still limited compared to the classical phases like lamellae, cylinders, and spheres.

Among the equilibrium ordered phases, a rich variety of reversible order−order phase transitions (OOTs), such as cylinders-to-spheres,[10−14] lamellae-to-cylinders,[14,15] cylinders-to-gyroid,[16−25] and lamellae-to-gyroid,[20,24,26−32] have been observed experimentally and were described theoretically. These OOTs can be induced by alteration of temperature, addition of homopolymers, introduction of selective solvents, or by application of external fields such as flow or electric fields. Honda and Kawakatsu studied the transition from the gyroid structure into hexagonally packed cylinders induced by an external shear flow by means of self-consistent-field theory.[21] Nonomura et al. studied the transition of the gyroid structure into lamellar and hexagonal cylindrical structures using the amplitude equations.[24] Matsen described gyroid-to-cylinder transitions under temperature change with self-consistent-field theory.[25] Recently, Zvelindovsky et al. showed electric field induced gyroid-to-cylinder transitions using self-consistent-field theory and cell dynamics simulations.[22,23]

In addition to the above-described theoretical work, Eskimergen et al. studied the stability of the gyroid structure using combined oscillated shear and small-angle neutron scattering techniques.[18] They showed that the gyroid phase of a polystyrene-*b*-polyisoprene diblock copolymer is unstable when exposed to large-amplitude high-frequency shear deformation. Under a shear flow in the [111] direction of the gyroid unit cell, a nucleation and growth of the cylinder domains was observed. The gyroid arms perpendicularly oriented to the flow direction do not contribute to the formation of the cylindrical domains; i.e., they vanish during the transition. On the other hand, those that are nearly parallel to the [111] direction are elongated by the shear flow and transformed into cylinders.[18,21] Application of another type of field, e.g. electric field, will most likely change the nature of the transition.

So far, there are only few experimental studies on electric field induced OOTs in thin films. Xu et al. found that the spherical microdomains of an asymmetric diblock copolymer were deformed into ellipsoids under an electric field and, with time, interconnected to cylindrical microdomains oriented in the direction of the applied electric field.[33] Crossland et al. studied the influence of an electric field on a gyroid forming block copolymer thin film. They observed vertical arrays of cylinders, lamellae, perforated lamellae, and gyroid phases depending on the temperature and the polymer−substrate interaction.[34]

*Corresponding author. E-mail: boeker@dwi.rwth-aachen.de.

 Published on Web 04/14/2010

Furthermore, the influence of an electric field on the order−disorder transition temperature was described recently.[35] In addition, the orientation of both lamellar and cylindrical microdomain structures by virtue of a dc electric field is studied extensively.[36−45] The driving force for the reorientation of microdomain structures under an electric field is the electrostatic free energy penalty associated with the dielectric interfaces which are not parallel to the electric field vector. While the free energy penalty can be eliminated by reorientation of lamellae and cylinders, it cannot be eliminated in cubic phases, such as the gyroid or spherical phase. However, it can be reduced by distorting the phase. When a field is applied to lamellar or hexagonal phases, it exerts a torque which causes grain rotation. The torque is zero, and the energy at a minimum, when the lamellae or cylinders are oriented parallel to the field. The spherical and gyroid phases, on the other hand, always have dielectric interfaces that are not parallel to the field, and their free energy under the influence of an electric field is higher than without field. Hence, the structures elongate in the applied field direction, to an extent at which electrostatic and elastic forces are in equilibrium. The free energy of this distorted phase, whose symmetry is reduced, increases with respect to the other phases, a circumstance which can bring about a phase transition.[46,47]

In this paper, we describe the reversible, electric field induced gyroid-to-cylinder transition of a polystyrene-*b*-polyisoprene diblock copolymer. At low electric fields the gyroid phase becomes distorted and aligns in the direction of the electric field lines. The application of higher electric fields results in an order−order transition to the cylindrical phase where the cylinders are oriented in the field direction. After switching off the electric field a cylinder-to-gyroid transition occurs, leading to a highly oriented gyroid phase.

Methods

Synthesis. A polystyrene-*b*-polyisoprene block copolymer with a total number-average molecular weight M_w = 72 000 g/mol was synthesized by sequential living anionic polymerization as described previously.[48] The polymer used in this study consists of 69 wt % polystyrene and 31 wt % polyisoprene (92% 1,4-cis). In the following, the polymer will be denoted as $S_{69}I_{31}{}^{72}$. Gel permeation chromatography (GPC) of the final block copolymer yields a polydispersity of $M_w/M_n < 1.05$. The block ratio and overall molecular weight were determined by ^{1}H NMR using the integrated aromatic signals of the polystyrene block in combination with the GPC results of the corresponding polystyrene precursor.

Sample Preparation and Capacitor Setup. Toluene solutions of the block copolymer with a concentration of 45 wt % were prepared. The electric field experiments were carried out in a home-built capacitor at room temperature. The capacitor consists of two planar gold electrodes (5×10 mm^2) with a spacing of 1 mm embedded in a Teflon block with two glass windows (perpendicular to the electrodes in the direction of the X-ray beam). The sample volume is large compared to the volume detected by the X-ray beam (100×100 μm^2) to exclude any surface effects of the electrodes. The sample solution is introduced into the capacitor via a syringe inserted at one side of the cell with an intake diameter corresponding to the electrode distance. After filling, the capacitor is closed with two Teflon screws. A dc voltage of up to 11 kV was applied across the capacitor, resulting in a homogeneous electric field pointing perpendicular to the X-ray beam direction (see Figure 2a). Both the voltage at the electrodes and the current through the sample were monitored during the course of the experiment. Since we did not detect any current during the measurements, we can exclude any effect caused by mobile ions in the system.

Small-Angle X-ray Scattering. Synchrotron SAXS measurements were performed at the ID02 beamline at the European Synchrotron Radiation Facility (ESRF, Grenoble, France). The diameter of the X-ray beam was 100 μm. The photon energy was set to 12.5 keV, corresponding to a wavelength of 0.1 nm. SAXS patterns were recorded with a two-dimensional CCD camera located at a distance of 10 m from the sample within an evacuated flight tube. The detector is capable of acquiring up to 120 frames (2048 × 2048 pixels) at a rate of 3 frames/s. Before data analysis, background scattering was subtracted from the data, and corrections were made for spatial distortions and for the detector efficiency.

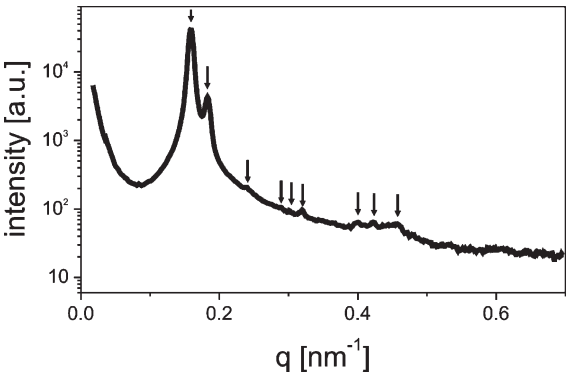

Figure 1. Scattering profile of a 45 wt % solution of $S_{67}I_{33}{}^{72}$ in toluene. The arrows identify the characteristic gyroid reflections.

To determine the exact peak position of the first-order Bragg peak in the direction parallel and perpendicular to the electric field lines, we averaged the corrected two-dimensional SAXS data over a 30° opening angle in the horizontal direction (parallel to the electric field lines) and the vertical direction (perpendicular to the field lines). The peak position in the scattering vector q was analyzed with a Voigt fitting model. The lattice distances were calculated according to $d_{hkl} = 2\pi/q_{hkl}$.

Results and Discussion

Phase Behavior without Electric Field. Before we discuss the effects of electric fields on the microdomains, we first concentrate on the microdomain structure, formed in a 45 wt % solution of $S_{69}I_{31}{}^{72}$ in toluene in the absence of an electric field. Toluene was chosen as solvent as it is fairly nonselective for PS and PI.[49] The polymer concentration was adjusted to be 2 wt % above the order−disorder concentration. Figures 1 and 2 show the scattering profile and 2D scattering pattern as well as the azimuthal scattering intensity dependence for this system. The SAXS profile exhibits nine reflections which are listed in Table 1. The relative positions of these peaks belong to the series $n^{1/2}q$ = 3, 4, 7, 10, 11, 12, 19, 21, and 25 as indicated by arrows in Figure 1. This sequence of observed reflections can be indexed as shown in Table 1 and can be attributed to the gyroid phase. The 10-to-1 intensity ratio between the first and second peak is consistent with that calculated and observed for the bicontinuous $Ia\bar{3}d$ morphology.[50]

On closer examination an anisotropic intensity distribution of the first-order Bragg peak was found as shown in Figure 2b. The scattering pattern of a gyroid structure was indexed previously by Förster et al.[51] and Vigild et al.[16] They examined the scattering pattern arising from a single crystal with the [111] lattice direction aligned perpendicular to the X-ray beam. By rotation of the single crystal around the [111] lattice direction, they determined different first-order spots depending on the orientation of the other lattice directions. The scattering from, for example, a single crystal with the [20$\bar{2}$] lattice direction aligned parallel to the X-ray beam gives a pair of meridional ⟨211⟩ reflections at ±90° and another

pair of ⟨211⟩ reflections at −19.5° and 160.5° with respect to the [111] equator. A 2D powder made up of domains rotated randomly around the [111] lattice direction results in the characteristic 10 first-order spots pattern observed for many gyroid structures. We observe four main spots in our $S_{69}I_{31}{}^{72}$ system at 74°, 179°, 257°, and 359° with respect to the normal of the electrode plane. If we assume the [111] lattice direction to be perpendicular to the normal of the electrodes, they can be assigned to 164°, 269°, 347°, and 89° with respect to the normal of the [111] lattice direction. The scattering pattern is similar to the pattern described above; i.e., the spots at 269° and 89° correspond to the ⟨211⟩ reflections at ±90°, whereas the spots at 164° and 347° relate to the ⟨211⟩ reflections at −19.5° and 160.5°. Therefore, we can conclude that the majority of the domains are oriented with the [111] lattice direction perpendicular to the normal of the electrodes and to the X-ray beam whereas the [20$\bar{2}$] lattice direction is aligned parallel to the X-ray beam, as illustrated in Figure 2a,c. This orientation may arise from shear forces occurring during the filling procedure as observed for lamellar systems previously.[40] As mentioned earlier, the sample solution is filled into the capacitor via a syringe leading to a shear field along the flow direction, i.e., perpendicular to the normal of the electrodes.

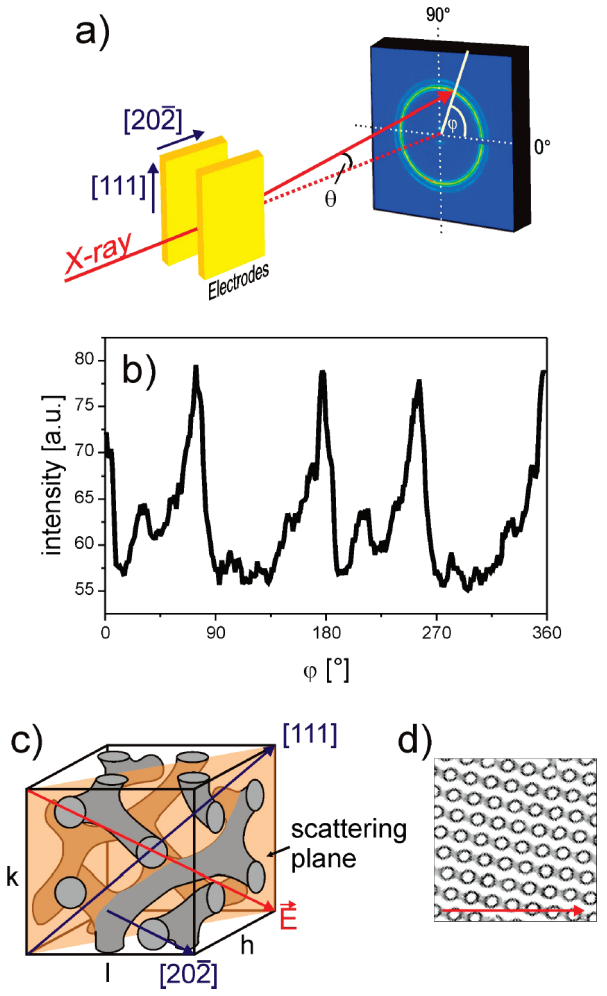

Figure 2. (a) 2D scattering pattern and experimental setup with respect to the geometry of the electric field and the X-ray beam. (b) Azimuthal dependence of the scattering intensity of the pattern shown in (a). (c) Schematic depiction of a gyroid structure with indication of the lattice directions, the scattering plane, and the electric field direction before alignment. The orientation of the lattice directions is shown in (a). (d) Cross section of the scattering plane; the arrow indicates the electric field direction.

Realignment of the Gyroid Phase with a Moderate Electric Field. First experiments were performed with moderate electric field strengths up to 6 kV/mm. We observed only slight differences in the overall scattering profile as shown in Figure 3a; i.e., the peak positions remain the same, indicating that the gyroid morphology is intact for all investigated electric field strengths up to 6 kV/mm. However, if we study the orientational behavior of the first-order Bragg peak, we find a different orientation of the gyroid structure under the influence of 6 kV/mm compared to the initial structure without a field. Figure 3b shows the azimuthal angular dependence of the scattering intensity for different electric field strengths. Clearly, there is no difference in the orientation up to 4 kV/mm. The pattern starts to change at 5 kV/mm, and for 6 kV/mm we find two distinct peaks at 90° and 270°. Figure 3c shows the evolution of the azimuthal angular dependence under the influence of a constant field of 6 kV/mm within the first minutes after application of the electric field. The initial peaks at 179° and 359° decrease whereas the initial peaks at 74° and 257° shift to 90° and 270° and grow with time. Such a pattern is expected from orientations where the [2$\bar{1}\bar{1}$] and [3$\bar{2}\bar{1}$] crystal planes are parallel with the scattering plane and the [111] lattice direction is parallel to the electric field lines, i.e., parallel to the normal of the electrodes and perpendicular to the X-ray beam as depicted in Figure 4.[16] This behavior indicates an electric field driven realignment of the gyroid structure. The destruction of the initial peaks at 179° and 359° and both the shift and the growth of the peaks at 74° and 257° show that gyroid domains, which are already orientated with the [111] lattice direction slightly parallel to the electric field, rotate in the field direction and then grow at the expense of those orientated perpendicular to the field direction. The energy required to rotate whole misaligned domains is too high. As a result, the growth mechanism proceeds rather via grain boundary migration which was observed already for lamella systems.[37]

Table 1. Comparison of Observed Reflections for a 45 wt % Solution of Polystyrene-*b*-polyisoprene ($S_{67}I_{33}{}^{72}$) in Toluene with Those Predicted for a Gyroid Structure

predicted		observed	predicted		observed
relative peak position ($n^{1/2}q$)	(hkl)	relative peak position ($n^{1/2}q$)	relative peak position ($n^{1/2}q$)	(hkl)	relative peak position ($n^{1/2}q$)
3	(211)	3	15	(521)	
4	(220)	4	16	(440)	
7	(321)	7	19	(611)	19
8	(400)		20	(620)	
10	(420)	10	21	(541)	21
11	(332)	11	23	(631)	
12	(422)	12	24	(444)	
13	(431)		25	(543)	25

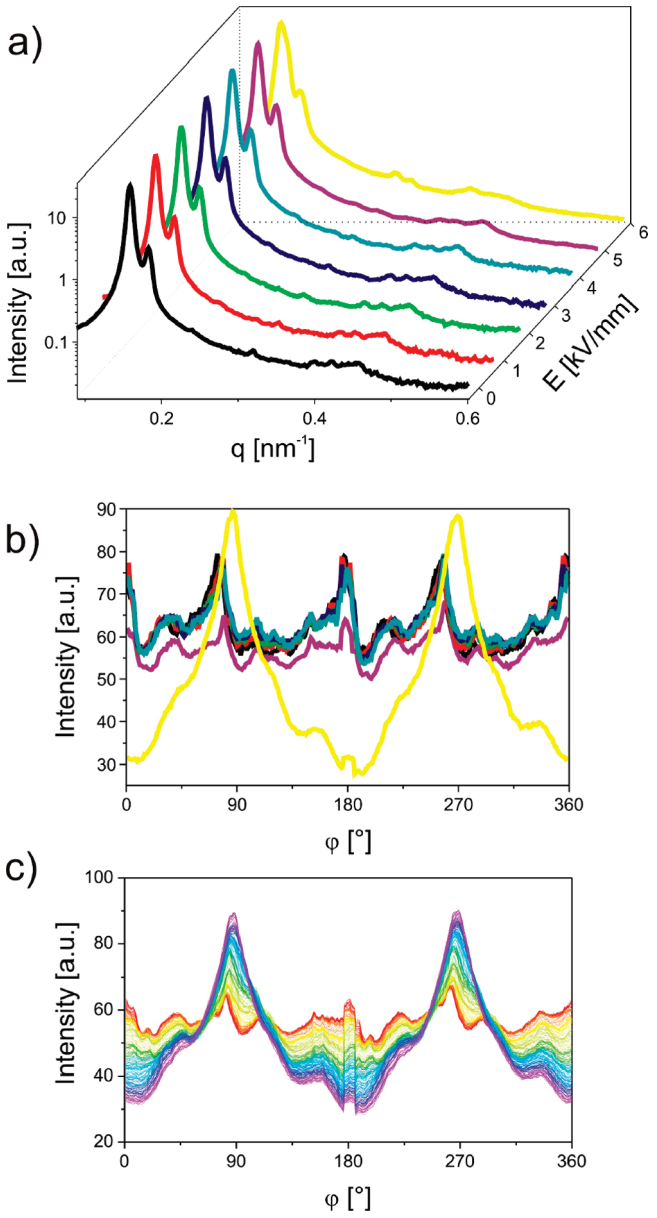

Figure 3. (a) Scattering profiles in dependence of the applied electric field strength. (b) Azimuthal angular dependence of the scattering intensity for different electric field strength. The colors correspond to the colors in (a). (c) Evolution of the azimuthal angular dependence under the influence of a constant field of 6 kV/mm with time, whereas red corresponds to $t = 0$ and purple to $t = 780$ s.

As mentioned above, the driving force for an electric field driven reorientation is in general the electrostatic free energy penalty arising from dielectric interfaces which are not parallel to the electric field lines. The free energy penalty can be reduced by reorientation of lamellae or cylinders, but not by reorientation of cubic phases, since every orientation has interfaces perpendicular to the electric field lines which is associated with a free energy penalty. Tsori et al. suggest a distortion of the cubic phases under electric fields. The structure elongates in the applied field direction and therefore can be aligned by the electric field.[46,47] Indeed, by closer examination of the scattering profile, we find different lattice distances for the gyroid structures depending on their orientation with respect to the electric field vector. Figure 5 shows the lattice distance d_{220} of gyroid structures which are aligned parallel to the electric field lines and those oriented perpendicular to the field lines.

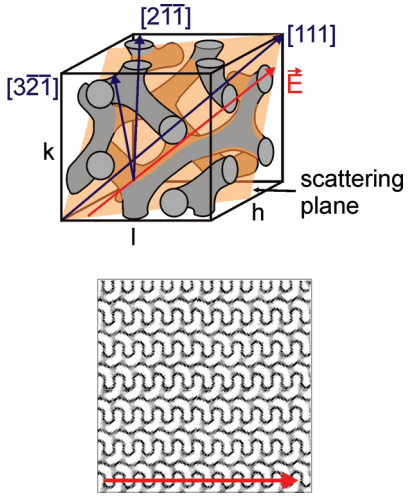

Figure 4. Schematic depiction of a gyroid structure (top) and cross section of the scattering plane (bottom) with indication of the lattice directions, the scattering plane, and the electric field direction after alignment with 6 kV/mm, as shown in Figure 3c.

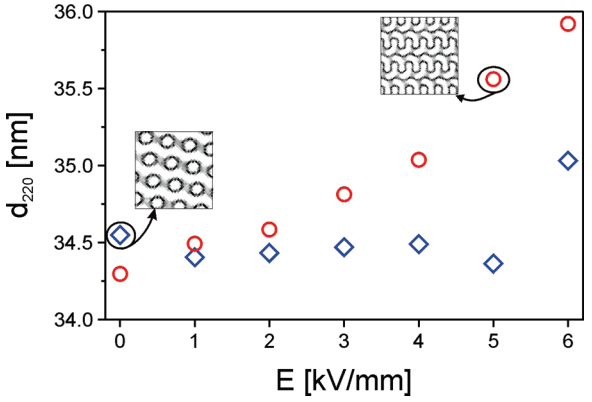

Figure 5. Lattice distance d_{220} of the gyroid structure with the [111] lattice direction parallel to the field lines (red circles) and perpendicular to the field lines (blue diamonds) in dependence of the electric field strength.

The lattice distance was calculated from the position of the second-order Bragg peak for different sectors of the scattering pattern as described in the experimental section. Up to 5 kV/mm we find no dependence of the gyroid lattice distances for structures with the [111] lattice direction perpendicular to the field lines. If the [111] lattice direction was parallel to the field lines, we observed an increase of the lattice distance with increasing electric field strength, indicating an electric field induced elongation of the gyroid morphology. As soon as we apply 6 kV/mm, the gyroid lattice distance of structures with the [111] lattice direction perpendicular to the field lines starts to increase as well. This behavior may be explained by (i) the reorientation of the gyroid structure which was already elongated by the electric field and (ii) the onset of the order−order transition to cylinders.

Gyroid-to-Cylinder Transition under Influence of a Strong Electric Field. After realignment with moderate electric field strengths the electric field was stepwise increased to 11 kV/mm. Prior to the SAXS measurements the system was equilibrated at the given electric field for 10 min. We observe a dramatic change in the overall scattering pattern as shown in Figure 6. A new reflection appears in the inner circle of the first-order Bragg peak at $0.8q^*$ (indicated by an arrow). This

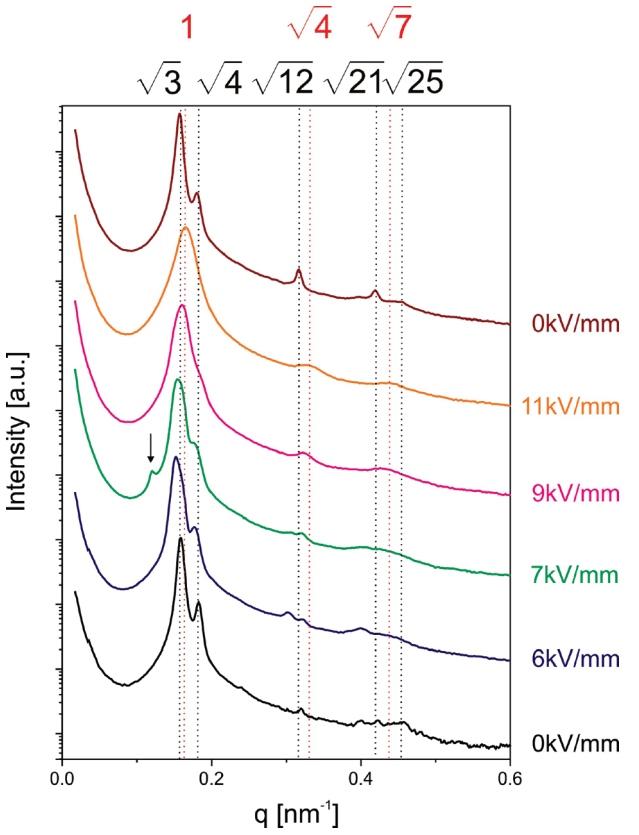

Figure 6. Overall scattering profiles in dependence of the applied electric field strength. The characteristic reflection for a gyroid structure (black) and a cylindrical structure (red) are indexed. The arrow indicates the new reflection at $0.8q^*$ arising from an intermediate morphology.

reflection is more distinct in the direction of the electric field than perpendicular to it. With further increase of the electric field up to 9 kV/mm the new reflection vanishes as well as the characteristic gyroid diffraction peaks, and we observe diffraction peaks at a ratio of 1:2:$\sqrt{7}$ which are characteristic for hexagonal structures.

The vanishing of these peaks depends on the orientation of the structure with respect to the electric field lines. Figure 7 shows the scattering profiles for gyroid structures which are aligned parallel to the field direction and for those oriented perpendicular to the electric field. The majority of the gyroid domains were aligned parallel to the electric field lines, and for these we mainly found diffraction peaks at a ratio of 1:2:$\sqrt{7}$. On the other hand, we still observe the gyroid reflections for those structures which were not aligned parallel to the electric field. However, these reflections also vanish with further increasing electric field strength up to 11 kV/mm, and only peaks at a ratio of 1:2:$\sqrt{7}$ could be identified for all orientations. We can explain this behavior by a phase transition from the gyroid to the cylindrical phase due to the influence of a high electric field. As pointed out before, it is not possible for the gyroid phase to eliminate the electrostatic energy penalty arising from dielectric interfaces in the electric field by reorientation. It was shown that the gyroid phase becomes distorted to lower the electrostatic energy penalty. Thus, the free energy of the elongated gyroid structure increases with increasing electric field strength. If the electric field is sufficiently high, the cylindrical phase is energetically favored, and the gyroid phase undergoes a phase transition to cylinders. These can be aligned parallel to the electric field lines, thereby eliminating the electrostatic energy penalty.

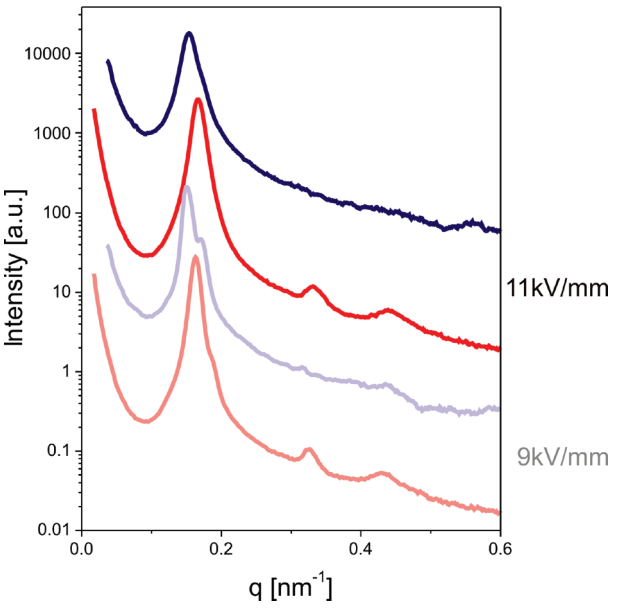

Figure 7. Scattering profiles of gyroid structures with the [111] lattice direction parallel to the field lines (red) and perpendicular to the field lines (blue) for electric field strengths of 9 kV/mm (light color) and 11 kV/mm (dark color).

Different pathways for the gyroid-to-cylinder transition were reported in the literature. Matsen proposed that the temperature-induced transition is initiated by the formation of a 5-fold junction from one 3-fold junction of the gyroid phase. Next its original three connections rupture, leaving a cylindrical unit connecting two distant 4-fold junctions. These transform into 5-fold junctions, and then their original connections break increasing the length of the cylinder (Figure 8). Repeating this process causes the lattice of the gyroid to completely unzip into cylinders.[25] The gyroid-to-cylinder transition under an electric field was investigated by Pinna et al. using cell dynamics simulations.[23] A similar pathway as proposed by Matsen was found. They reported that first the gyroid structure becomes stretched under the electric field. Then, the gyroid connections, which are perpendicular to the electric field lines, break, and the system transforms to helically wound cylinders. As time proceeds, these cylinders straighten.

On the other hand, the hexagonally perforated lamellar (HPL) phase is a common transient structure in the pathway of gyroid-to-lamellae transition and was also observed experimentally in the shear induced cylinder-to-gyroid transition by Imai et al.[32,52] The HPL phase consists of planar tripods and can be generated from the gyroid phase by rotating the dihedral angle of the connecting tripods. However, the hexagonally perforated lamellar structure was never observed in the reverse gyroid-to-cylinder transition.

On the basis of our scattering data, we cannot decide which pathway the gyroid-to-cylinder transition follows. We can, however, conclude that the new reflection, which appears at an electric field strength of 7 kV/mm, arises from an intermediate structural element exclusively existing during the early state of the gyroid-to-cylinder transition. In addition, we found that gyroid structures which are aligned with the [111] lattice direction parallel to the field lines first undergo a phase transition (see Figure 7). The energy needed to transform gyroid structures which could not be aligned is much higher, and the phase transition for those structures occurs at increased electric field strengths. These results are corroborated by dynamical self-consistent-field theory

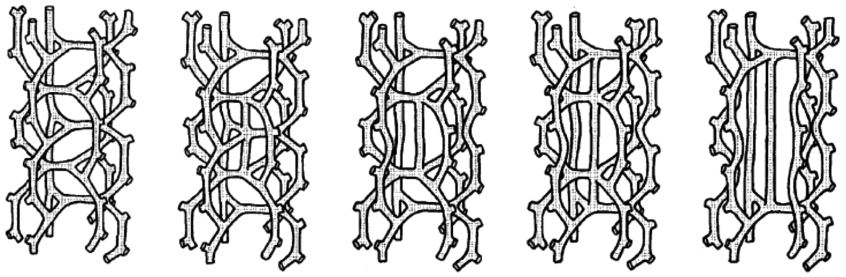

Figure 8. Schematic illustration of the gyroid-to-cylinder transition as proposed by Matsen. Reprinted with permission from ref 25. Copyright 1998 American Physical Society.

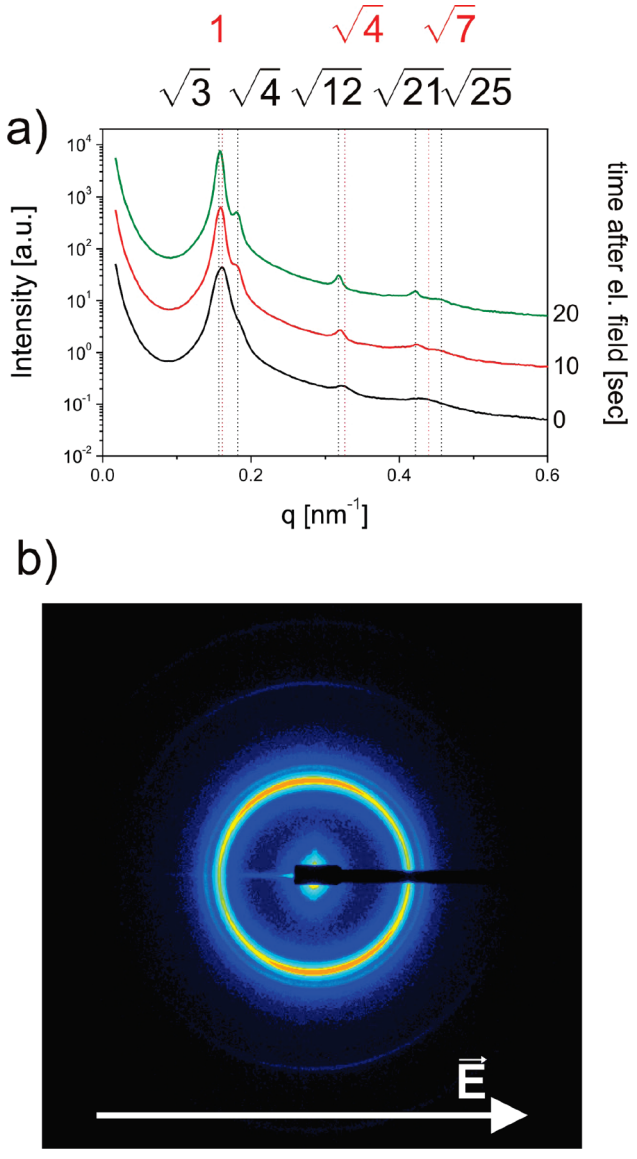

Figure 9. (a) Evolution of the scattering profile after switch-off of the electric field (9 kV/mm) with time. The characteristic reflections for a gyroid structure (black) and a cylindrical structure (red) are indexed. (b) 2D scattering pattern after 160 s after switch-off of the electric field. The arrow indicates the electric field direction.

studies of the shear field induced gyroid-to-cylinder transition simulated by Honda et al.[21] They found that gyroid domains, which are oriented perpendicular to the shear direction, do not contribute to the formation of the cylindrical domains. They are disconnected and vanish during the transition. On the other hand, the gyroid domains parallel to the shear direction become elongated and transform into cylindrical domains.

Relaxation to the Gyroid Phase after Switch-Off of the Electric Field. As soon as the electric field is switched off, the original gyroid reflections appear again (Figure 6). Figure 9a shows the time evolution of the scattering profile after switch-off of the electric field. Clearly, a transition from the cylindrical phase to the gyroid phase is observed which proceeds within some seconds. In addition, we found no further peaks during the transition. If we examine the 2D scattering image after the switch-off, we observe a highly anisotropic pattern (Figure 9b). This pattern indicates that the gyroid structure is aligned perpendicular to the electrodes, i.e., parallel to the former electric field lines. We calculated an order parameter of $P_2 = -0.33$ as described elsewhere.[40] P_2 ranges from 1 to -0.5 with $P_2 = -0.5$ corresponding to a gyroid structure perfectly aligned parallel to the electric field lines and $P_2 = 1$ corresponding to structures fully aligned perpendicular to the electric field vector.

If the electric field is decreased, the free energy of the gyroid phase again becomes lower than the free energy of the cylindrical phase. Thus, a cylinder-to-gyroid transition occurs with the switch-off of the electric field. This transition proceeds rather fast, which indicates furthermore that the cylindrical structure is not stable without an electric field. As explained above, the gyroid-to-cylinder transition is expected to proceed via an intermediate HPL phase or via 4- and 5-fold junctions within the gyroid phase. For both pathways an extra reflection arising from the intermediate structure is expected. The absence of any transient peaks during the cylinder-to-gyroid transition suggests a different pathway with no intermediate morphology. Vilgid et al. observed an epitaxial hexagonal-to-gyroid transition without any transient structure by a shallow temperature quench of the hexagonal phase.[16] They also point to the fact that with increasing stability of the final structure the transition is more likely to proceed via intermediate morphologies. In addition, the final gyroid structure is aligned parallel to the former electric field lines. As it is known that the alignment of lamellae or cylinders in an electric field is stable even after the electric field is switched off,[38] this finding corroborates the suggested pathway above, since in the case of an epitaxial transition, the gyroid structure will be aligned in the same direction as the cylindrical structure.

Conclusion

In summary, we found a reversible gyroid-to-cylinder transition of a polystyrene-*b*-polyisoprene diblock copolymer system under the influence of a high electric field. We showed that the shear-aligned gyroid structure can be distorted and realigned by a moderate electric field. As the electric field is increased, the free energy of the gyroid increases and forces the system to undergo a

phase transition to the cylindrical phase. This cylindrical phase is unstable without an electric field, and as soon as the electric field is switched off, the cylinders undergo a phase transition back to the gyroid phase. Both transitions proceed via different pathways. The resulting gyroid phase is highly aligned in the direction of the former cylinder orientation.

Acknowledgment. The authors thank H. Krejtschi and his team for the assistance building the capacitors, H. Hänsel, F. Schubert, F. Fischer, E. Di Cola, M. Sztucki, and P. Bösecke for the help at the ESRF, and Y. Tsori and D. Andelman for fruitful discussions. We are grateful to the ESRF for provision of synchrotron beam time. K.S. thanks the Alexander-von-Humboldt foundation for sponsorship by the Feodor-Lynen postdoctoral program. A.B. acknowledges support by the Lichtenberg-Programm of the Volkswagen-Stiftung. This work was carried out in the framework of the Sonderforschungsbereich 481 (TP A2) funded by the German Science Foundation (DFG).

References and Notes

(1) Matsen, M. W.; Bates, F. S. *Macromolecules* **1996**, *29* (4), 1091–1098.
(2) Helfand, E.; Wasserman, Z. R. *Macromolecules* **1980**, *13* (4), 994–998.
(3) Fredrickson, G. H.; Helfand, E. *J. Chem. Phys.* **1987**, *87* (1), 697–705.
(4) Bates, F. S.; Fredrickson, G. H. *Annu. Rev. Phys. Chem.* **1990**, *41*, 525–557.
(5) Matsen, M. W.; Schick, M. *Phys. Rev. Lett.* **1994**, *72* (16), 2660–2663.
(6) Leibler, L. *Macromolecules* **1980**, *13* (6), 1602–1617.
(7) Edrington, A. C.; Urbas, A. M.; DeRege, P.; Chen, C. X.; Swager, T. M.; Hadjichristidis, N.; Xenidou, M.; Fetters, L. J.; Joannopoulos, J. D.; Fink, Y.; Thomas, E. L. *Adv. Mater.* **2001**, *13* (6), 421–425.
(8) Hashimoto, T.; Tsutsumi, K.; Funaki, Y. *Langmuir* **1997**, *13* (26), 6869–6872.
(9) Zhao, D. Y.; Feng, J. L.; Huo, Q. S.; Melosh, N.; Fredrickson, G. H.; Chmelka, B. F.; Stucky, G. D. *Science* **1998**, *279* (5350), 548–552.
(10) Kimishima, K.; Koga, T.; Hashimoto, T. *Macromolecules* **2000**, *33* (3), 968–977.
(11) Krishnamoorti, R.; Silva, A. S.; Modi, M. A.; Hammouda, B. *Macromolecules* **2000**, *33* (10), 3803–3809.
(12) Lee, H. H.; Jeong, W. Y.; Kim, J. K.; Ihn, K. J.; Kornfield, J. A.; Wang, Z. G.; Qi, S. Y. *Macromolecules* **2002**, *35* (3), 785–794.
(13) Pinna, M.; Zvelindovsky, A. V.; Todd, S.; Goldbeck-Wood, G. *J. Chem. Phys.* **2006**, *125* (15), 154905.
(14) Lyakhova, K. S.; Zvelindovsky, A. V.; Sevink, G. J. A. *Macromolecules* **2006**, *39* (8), 3024–3037.
(15) Hajduk, D. A.; Harper, P. E.; Gruner, S. M.; Honeker, C. C.; Kim, G.; Thomas, E. L.; Fetters, L. J. *Macromolecules* **1994**, *27* (15), 4063–4075.
(16) Vigild, M. E.; Almdal, K.; Mortensen, K.; Hamley, I. W.; Fairclough, J. P. A.; Ryan, A. J. *Macromolecules* **1998**, *31* (17), 5702–5716.
(17) Schulz, M. F.; Bates, F. S.; Almdal, K.; Mortensen, K. *Phys. Rev. Lett.* **1994**, *73* (1), 86–89.
(18) Eskimergen, R.; Mortensen, K.; Vigild, M. E. *Macromolecules* **2005**, *38* (4), 1286–1291.
(19) Wang, C. Y.; Lodge, T. P. *Macromolecules* **2002**, *35* (18), 6997–7006.
(20) Yu, B.; Li, B. H.; Sun, P. C.; Chen, T. H.; Jin, Q. H.; Ding, D. T.; Shi, A. C. *J. Chem. Phys.* **2005**, *123* (23).
(21) Honda, T.; Kawakatsu, T. *Macromolecules* **2006**, *39* (6), 2340–2349.
(22) Ly, D. Q.; Honda, T.; Kawakatsu, T.; Zvelindovsky, A. V. *Macromolecules* **2007**, *40* (8), 2928–2935.
(23) Pinna, M.; Zvelindovsky, A. V. *Soft Matter* **2008**, *4* (2), 316–327.
(24) Nonomura, M.; Yamada, K.; Ohta, T. *J. Phys.: Condens. Matter* **2003**, *15* (26), L423–L430.
(25) Matsen, M. W. *Phys. Rev. Lett.* **1998**, *80* (20), 4470–4473.
(26) Schmidt, S. C.; Hillmyer, M. A. *J. Polym. Sci., Part B: Polym. Phys.* **2002**, *40* (20), 2364–2376.
(27) Hamley, I. W.; Fairclough, J. P. A.; Ryan, A. J.; Mai, S. M.; Booth, C. *Phys. Chem. Chem. Phys.* **1999**, *1* (9), 2097–2101.
(28) Sakurai, S.; Umeda, H.; Furukawa, C.; Irie, H.; Nomura, S.; Lee, H. H.; Kim, J. K. *J. Chem. Phys.* **1998**, *108* (10), 4333–4339.
(29) Hajduk, D. A.; Ho, R. M.; Hillmyer, M. A.; Bates, F. S.; Almdal, K. *J. Phys. Chem. B* **1998**, *102* (8), 1356–1363.
(30) Park, I.; Lee, B.; Ryu, J.; Im, K.; Yoon, J.; Ree, M.; Chang, T. *Macromolecules* **2005**, *38* (25), 10532–10536.
(31) Hamley, I. W.; Castelletto, V.; Mykhaylyk, O. O.; Yang, Z.; May, R. P.; Lyakhova, K. S.; Sevink, G. J. A.; Zvelindovsky, A. V. *Langmuir* **2004**, *20* (25), 10785–10790.
(32) Imai, M.; Saeki, A.; Teramoto, T.; Kawaguchi, A.; Nakaya, K.; Kato, T.; Ito, K. *J. Chem. Phys.* **2001**, *115* (22), 10525–10531.
(33) Xu, T.; Zvelindovsky, A. V.; Sevink, G. J. A.; Gang, O.; Ocko, B.; Zhu, Y. Q.; Gido, S. P.; Russell, T. P. *Macromolecules* **2004**, *37* (18), 6980–6984.
(34) Crossland, E. J. W.; Ludwigs, S.; Hillmyerd, M. A.; Steiner, U. *Soft Matter* **2009**, *6*, 670–676.
(35) Schoberth, H. G.; Schmidt, K.; Schindler, K. A.; Boker, A. *Macromolecules* **2009**, *42* (10), 3433–3436.
(36) Amundson, K.; Helfand, E.; Quan, X. N.; Hudson, S. D.; Smith, S. D. *Macromolecules* **1994**, *27* (22), 6559–6570.
(37) Böker, A.; Elbs, H.; Hänsel, H.; Knoll, A.; Ludwigs, S.; Zettl, H.; Urban, V.; Abetz, V.; Müller, A. H. E.; Krausch, G. *Phys. Rev. Lett.* **2002**, *89* (13), 135502.
(38) Böker, A.; Elbs, H.; Hänsel, H.; Knoll, A.; Ludwigs, S.; Zettl, H.; Zvelindovsky, A. V.; Sevink, G. J. A.; Urban, V.; Abetz, V.; Müller, A. H. E.; Krausch, G. *Macromolecules* **2003**, *36* (21), 8078–8087.
(39) Böker, A.; Schmidt, K.; Knoll, A.; Zettl, H.; Hänsel, H.; Urban, V.; Abetz, V.; Krausch, G. *Polymer* **2006**, *47* (3), 849–857.
(40) Schmidt, K.; Böker, A.; Zettl, H.; Schubert, F.; Hänsel, H.; Fischer, F.; Weiss, T. M.; Abetz, V.; Zvelindovsky, A. V.; Sevink, G. J. A.; Krausch, G. *Langmuir* **2005**, *21* (25), 11974–11980.
(41) Schmidt, K.; Schoberth, H. G.; Schubert, F.; Hansel, H.; Fischer, F.; Weiss, T. M.; Sevink, G. J. A.; Zvelindovsky, A. V.; Böker, A.; Krausch, G. *Soft Matter* **2007**, *3* (4), 448–453.
(42) Xu, T.; Hawker, C. J.; Russell, T. P. *Macromolecules* **2003**, *36* (16), 6178–6182.
(43) Xu, T.; Zhu, Y. Q.; Gido, S. P.; Russell, T. P. *Macromolecules* **2004**, *37* (7), 2625–2629.
(44) Xu, T.; Zvelindovsky, A. V.; Sevink, G. J. A.; Lyakhova, K. S.; Jinnai, H.; Russell, T. P. *Macromolecules* **2005**, *38* (26), 10788–10798.
(45) Olszowka, V.; Hund, M.; Kuntermann, V.; Scherdel, S.; Tsarkova, L.; Böker, A.; Krausch, G. *Soft Matter* **2006**, *2*, 1089–1094.
(46) Tsori, Y.; Tournilhac, F.; Andelman, D.; Leibler, L. *Phys. Rev. Lett.* **2003**, *90* (14), 145504/145501–145504/145504.
(47) Tsori, Y.; Andelman, D.; Lin, C. Y.; Schick, M. *Macromolecules* **2006**, *39* (1), 289–293.
(48) Schmalz, H.; Böker, A.; Lange, R.; Krausch, G.; Abetz, V. *Macromolecules* **2001**, *34* (25), 8720–8729.
(49) Huang, C. I.; Chapman, B. R.; Lodge, T. P.; Balsara, N. P. *Macromolecules* **1998**, *31* (26), 9384–9386.
(50) Luzzati, V.; Spegt, P. A. *Nature* **1967**, *215* (5102), 701.
(51) Förster, S.; Khandpur, A. K.; Zhao, J.; Bates, F. S.; Hamley, I. W.; Ryan, A. J.; Bras, W. *Macromolecules* **1994**, *27* (23), 6922–6935.
(52) Imai, M.; Sakai, K.; Kikuchi, M.; Nakaya, K.; Saeki, A.; Teramoto, T. *J. Chem. Phys.* **2005**, *122* (21), 214906.